Real Space Structure and Scattering Patterns of Model Polymer Nanocomposites

Justin B. Hooper[†] and Kenneth S. Schweizer*

Departments of Materials Science and Engineering, University of Illinois, 1304 West Green Street, Urbana, Illinois 61801

Received May 21, 2007; Revised Manuscript Received July 10, 2007

ABSTRACT: Microscopic polymer liquid state theory is employed to study the real space pair correlation functions and collective scattering structure factors of melt polymer nanocomposites composed of hard spheres and adsorbing homopolymers over length scales ranging from monomeric to macroscopic. Increasing filler volume fraction has a profound effect on the polymer matrix, inducing oscillatory reorganization on a length scale commensurate with the nanoparticle diameter. The near contact interfacial monomer−filler pair correlations are suppressed by nanoparticle addition, but on larger scales power law correlations emerge with filler imprinted oscillatory features. Increased nanoparticle volume fraction also substantially changes interfiller packing, inducing a transition from a highly bridged or sterically stabilized type of organization in the infinite dilution limit to more diffuse liquidlike packing characterized by many-particle clustering. Distinctive modifications of the collective polymer structure factor include an increase in the osmotic compressibility, the emergence of a large bound layer or microphase-separation-like scattering peak on a length scale controlled by filler size indicative of distinct bound polymer layers, and a local rarefaction and suppression of the coherence of the monomer cage scale packing. All the real and Fourier space correlations depend in distinctive manners on the physical and chemical variables (filler size, volume fraction, strength and spatial range of the interfacial cohesion) and proximity to the contact aggregation and bridging phase separation boundaries. The bulk modulus of the nanocomposite generically softens with the addition of fillers corresponding to enhanced total density fluctuations.

I. Introduction

The structure, phase behavior, and thermomechanical properties of dense fluid and solid mixtures of polymers and particles are of major scientific and technological interest.[1−5] Diverse theoretical and simulation approaches have begun to be employed to study the elementary equilibrium, and to a lesser extent viscoelastic, properties of model polymer nanocomposites (PNC).[6−23] Major computational difficulties are associated with direct computer simulations under high particle volume fraction and realistic particle−monomer diameter ratio conditions due to the presence of a wide range of relevant length and time scales and the need for long equilibration runs. In a series of recent publications,[17−19] we have developed and applied a microscopic polymer reference interaction site model (PRISM) integral equation theory[24] to systematically investigate structure, filler potential of mean force (PMF), thermodynamics, and miscibility in the dilute one- and two-particle limit. A broad range of interfacial adsorption, chain length, and particle size conditions have been examined. The complex and competing consequences of entropic packing and enthalpic considerations of both interfacial (polymer−particle) and direct (particle−particle) attraction origin on the filler PMF, monomer−particle pair correlations, and virial coefficients have been established. Comparisons of the PRISM calculations with computer simulations for both athermal and adsorbing polymers suggest the theory is quite accurate.[8,17,20] Most recently, a PRISM study of mixtures of hard fillers and star polymers has been performed.[21]

Figure 1 presents a schematic summary of the prior PMF and spinodal phase boundary studies for hard-sphere fillers.[17−19]

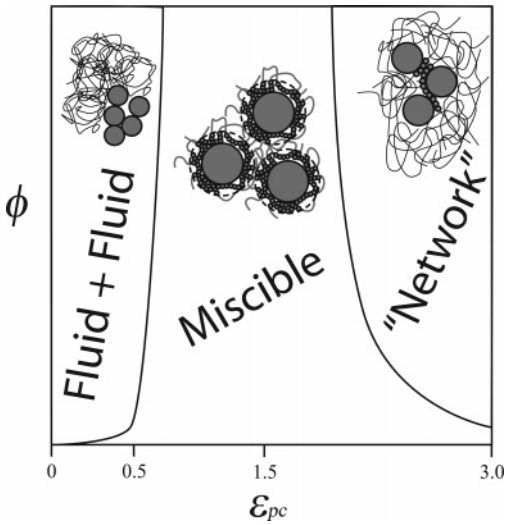

Figure 1. Schematic representation of the generic polymer nanocomposite phase behavior. At low ϵ_{pc} (in units of k_BT) traditional fluid + fluid phase separation occurs, while at median ϵ_{pc}values adsorption of polymer onto the nanoparticle provides a thin bound layer that results in steric stabilization and miscibility. For high interfacial energies the adsorbed monomers associate with multiple nanoparticles, leading to a bridging-induced "network"-like phase.

The contact strength (ϵ_{pc}, in units of the thermal energy k_BT) and spatial range (αd, where d is the monomer diameter) of monomer−particle attraction, and the filler−monomer diameter ratio (D/d), are key variables. The degree of polymerization (N) has been found to play a relatively minor role as expected under equilibrium high-density conditions.[17−19] One limiting behavior is the entropically dominated (nearly) athermal system ($\epsilon_{pc} \ll k_BT$) where oscillatory depletion attractions favor contact particle aggregation. The other limit is an enthalpically dominated

* Corresponding author. E-mail: kschweiz@uiuc.edu.
[†] Present address : Department of Materials Science and Engineering, University of Utah, 122 S. Central Campus Dr., Rm 304, Salt Lake City, UT 84112.

10.1021/ma071147e CCC: $37.00
Published on Web 08/21/2007

regime where strong filler−monomer adsorption favors well-defined, small interparticle separations, i.e., local bridging. Between these two extremes is a third, compromise state of organization, in which a polymer gains enough cohesive interaction energy to associate with a single filler, but not enough to give up the additional entropy required for bridging with multiple particles. In this case a nanoparticle is surrounded by a *thermodynamically* stable "bound polymer layer", typically of order a few monomer diameters thick, which sterically stabilizes the fillers in the polymer matrix.[18] By "thermodynamically stable" we mean the equilibrium PMF is purely repulsive. This is in contrast to the classic kinetic stabilization mechanism where a large repulsive barrier in the PMF exists at interparticle separations beyond a strong very short range attraction which under true equilibrium conditions would favor particle aggregation.

On the basis of a virial analysis, the corresponding spinodal phase behavior has been established[19] and reflects the three categories of filler PMF summarized above. Two distinct demixing behaviors, separated by a miscibility window, are generically predicted, corresponding to a lower critical solution temperature (LCST) type of phase behavior. A demixing boundary occurs at relatively low monomer−particle attraction strength ($\epsilon_{pc} < 0.3-0.5\ k_BT$) and corresponds to an abrupt transition from an (athermal/high temperature) entropic depletion attraction induced state composed of polymer-rich and nanoparticle-rich phases to a homogeneous sterically stabilized miscible fluid. The location of this spinodal boundary is weakly sensitive to the size asymmetry ratio (D/d) and interfacial attraction range (α). The second demixing transition occurs at high monomer−particle adsorption energy or low relative temperature ($\epsilon_{pc} \sim 2-3\ k_BT$) and signals the dominance of enthalpic effects in the free energy of mixing. Its physical nature has been inferred to involve the formation of a thermodynamically stable networked phase where fillers are locally bridged by polymer chains. This spinodal boundary is more sensitive to D/d and α, with increases of either resulting in a narrowing of the range of parameter space over which miscibility occurs. Bridging is also quantitatively enhanced with increasing chain length. In practice, phase separation where the spatial organization of one of the coexisting phases of the PNC is a dense interpenetrating network or complex is likely very difficult to realize in the laboratory due to slow kinetics. Instead, strong bridging coupled with particle percolation likely triggers nonequilibrium physical network formation. Finally, at intermediate temperatures or interfacial cohesion strengths a miscibility window is predicted corresponding to the steric stabilization type of PMF. It systematically narrows, and can ultimately disappear, with increasing polymer chain length (a finite size effect), direct van der Waals attractions between fillers (due to dielectric constant mismatch of the filler and polymer matrix), and/or particle−monomer size asymmetry ratio D/d.[19] Experimental realization of thermodynamic dispersion thus requires both an intermediate value of ϵ_{pc} and modest sized nanofillers.

While much interesting behavior of polymer−particle mixtures can be investigated in the low particle concentration limit, with the advantages of conceptual and computational simplicity, in real nanocomposites there is a finite limit for the maximum distance a polymer chain may be from multiple fillers. As particle volume fraction increases, interference of macromolecular organization in the vicinity of different fillers must occur to an extent that depends on particle surface area and hence size. This "many-body effect" introduces new physics, the systematic elucidation of which is the focus of the present work. With the inclusion of many-body effects, the polymer−polymer, polymer−particle, and particle−particle pair correlation (or radial distribution) functions ($g_{cc}(r)$, $g_{pc}(r)$, and $g_{pp}(r)$) become coupled and acquire an explicit dependence on filler volume fraction, ϕ, and the multiple controllable chemical and physical variables (D/d, N, ϕ, α, ϵ_{pc}). One expects the consequences of increasing filler concentration will depend on the proximity of the nanocomposite to a demixing phase boundary, and distinctive phase separation precursor behaviors seem likely at high and low monomer−particle adsorption energies. Our theoretical characterization of the statistical structure will also include the corresponding partial structure factors in order to establish the scattering experiment signatures of real space correlations. Besides the shifting and intensity changes of local (cage scale) measures of organization with increasing filler volume fraction, new features emerge on the mesoscale indicative of macroscopic and microphase separation type behavior reminiscent of the behavior of some block copolymer and microemulsion systems.

In section II the model and PRISM theory are briefly summarized. Results for real space correlations and structure factors are presented and discussed in sections III and IV, respectively. Our goal is to provide a unified picture of structural pair correlations and their Fourier space signatures. Calculations of the mixture bulk modulus are given in section V, and the paper concludes in section VI with a brief summary and discussion.

II. Theory and Models

Technical details of the model and theory have been given in prior papers.[17−19] The statistical polymer conformation is assumed to be unperturbed by the presence of fillers. This simplification seems physically reasonable at the nearly incompressible melt conditions of interest, and experimental support has recently been obtained.[25,26]

Polymers are modeled as athermal, freely jointed chains (FJC) of N spherical interaction sites or monomers of diameter d which interact via pair decomposable hard-core potentials. The rigid bond (persistence) length $l = 4d/3$, where d is the polymer segment diameter which is taken as the unit of length. The FJC structure factor is[24,27]

$$\omega_p(k) = (1-f)^{-2}[1 - f^2 - 2N^{-1}f + 2N^{-1}f^{N+1}] \quad (1)$$

where $f \equiv \sin(kl)/kl$. Fillers are rigid spheres of diameter D which have a trivial single particle structure factor, $\omega_c(k) \equiv 1$. A minimalist, but rather realistic,[18,19] two-parameter monomer−particle attraction of an exponential form is utilized. It is defined by a strength at contact, ϵ_{pc}, and a dimensionless spatial range parameter α

$$U_{pc}(r) = -\epsilon_{pc} \exp\left[-\frac{r - \sigma_{pc}}{\alpha d}\right] \quad (2)$$

where $\sigma_{pc} = (D + d)/2$. For real materials the magnitude of ϵ_{pc} can vary from "weak" (a fraction of a k_BT) to strong (several k_BT).[18] Throughout the paper ϵ_{pc} and all other energies are in units of the thermal energy. The parameter α is also material-dependent and within a FJC model depends on the angstrom scale chemical details that have been averaged over (e.g., monomer size and shape). As previously discussed,[18] different values of α mimic the different types of intermolecular attractions experienced in real systems, with $\alpha \sim 0.25-1$ covering the range expected for chemically specific (shorter range) interactions to generic van der Waals attractions. Direct filler−filler attractions are not considered in the present work

although it is straightforward to include them. We note that direct van der Waals attractions favor filler aggregation and phase separation, and quantitative examples of their consequences on the dilute particle PMF[18] and virial-level spinodal phase diagrams[19] have been previously given. These prior results are expected to provide a qualitatively reliable indication of the direct attraction consequences at high filler volume fractions.

By treating all sites on a chain as statistically equivalent, the PNC PRISM theory is defined by three coupled nonlinear site−site Ornstein−Zernike-like integral equations. In Fourier transform space they are given by[17−19,24,28]

$$h_{ij}(k) = \omega_i[C_{ij}(k)\omega_j + \sum_l C_{il}(k)\rho_l h_{lj}(k)] \quad (3)$$

where $h_{ij}(r) = g_{ij}(r) - 1$ is the nonrandom part of the intermolecular site−site pair correlation function between species i and j, $C_{ij}(r)$ is the corresponding intermolecular direct correlation function, $\omega_i(k)$ is the single molecule structure factor of species i, and ρ_l is the site number density of species l. Hard-core interactions imply the exact impenetrability conditions:

$$g_{ij}(r) \equiv 0, \quad r < \sigma_{ij} \quad (4)$$

where σ_{ij} is the distance of closest approach between sites of type i and j. The site−site PY closure approximation[24,28] is adopted for the polymer−polymer (PP) and polymer−particle (PC) direct correlations:

$$C_{ij}(r) = (1 - e^{\beta U_{ij}(r)})g_{ij}(r), \quad r > \sigma_{ij} \quad (5)$$

where U_{ij} is the site−site interaction potential. The HNC closure is utilized for the $r > \sigma_{cc}$ particle−particle (CC) direct correlations:[28,29]

$$C_{cc}(r) = h_{cc}(r) - \ln g_{cc}(r) - \beta U_{cc}(r), \quad r > \sigma_{cc} \quad (6)$$

Prior work has demonstrated PRISM theory with the above closures accurately captures all features of the monomer−filler and particle−particle pair correlations in the dilute limit under dense melt conditions.[8,17,18,20] The dimensionless diagonal partial collective density fluctuation structure factors of interest are given by

$$S_{ii}(k) = \omega_i(k) + \rho_i h_{ii}(k) \quad (7)$$

In the present work all calculations are performed at a total packing fraction of $\eta = 0.4$, which corresponds to a typical dense liquid value and a realistic dimensionless compressibility.[18,24] The volumetric fraction of fillers in the mixture is denoted as ϕ. The integral equations are solved with the iterative Picard method.[29]

III. Real Space Pair Correlations

The parameters that define the model are polymer degree of polymerization (N), monomer−filler attraction (α, ϵ_{pc}), filler volume fraction (ϕ), and size asymmetry ratio (D/d). Since the degree of polymerization plays a minor role,[17−19] all presented calculations employ the representative value of $N = 100$. Filler volume fraction is varied from 0 to 0.40. Primarily three values of monomer−filler contact adsorption energy are studied: $\epsilon_{pc} = 0.5$ (relatively close to the contact aggregation phase boundary), 1 (well inside the sterically stabilized miscible regime), and 2 (approaching the bridging driven spinodal boundary).[18] The effect of monomer−particle attraction spatial range is quantitative, and calculations for $\alpha = 0.25$, 0.5, and 1 will be presented. Size asymmetry ratios in the range $D/d = 10-24$ have been studied with $D/d = 10$ taken as the default value. Since a polymer segment is of order 1 nm, this ratio corresponds to a 10 nm filler. We note that the location of the system state points studied relative to the virial-level spinodal boundaries is clear from the results in ref 19. However, the nondilute filler systems of present interest have corresponding spinodal boundaries that must quantitatively differ from their virial-based analogues. The full spinodal curves will be presented in a future publication based on a new numerical algorithm to solve the integral equations.

At nonzero filler volume fractions the pair correlation functions between any two components of the system (pp, pc, cc) depend in a highly coupled manner on all the system parameters. Besides the $g_{ij}(r)$'s, their explicitly nonrandom or correlated analog weighted by the appropriate surface area factor are also examined

$$\left(\frac{r}{r_c}\right)^2 h_{ij}(r) \quad (8)$$

where r_c is the distance of closest approach. This representation is especially useful for polymer correlations since it allows clear visualization of how fillers modify the local and long range (correlation hole scale $R_g = \sqrt{N/6}l$ and beyond) structure.

A. Polymer−Polymer Correlations. A common materials science motivation for creating a PNC is to strongly modify the properties of the polymer "matrix". The structural consequences of this are statistically characterized in real space by $g_{pp}(r)$. There are two primary length scales in a pure polymer melt. Local packing occurs on the monomer, d, and mesh, $\xi_\rho \sim d$, scale.[24,30] These features are generally strong at contact and decay relatively quickly in an oscillatory (period $\sim d$) manner. A universal long-range correlation hole exists[24,31] due to shielding of intermolecular chain contacts via intramolecular chain connectivity, i.e., $g_{pp}(r) < 1$ for $d \ll r < R_g$. For our prior infinite dilution filler work, the polymer pair correlations were rigorously unaffected by the nanoparticles. Hence, the influence of nonzero filler volume fraction on structure is most dramatic for the interchain correlations.

The reorganization of monomers necessary to accommodate fillers perturbs the normal polymer packing features and also introduces a new length scale. As can be seen in Figure 2, this occurs by an oscillatory "imprinting" of the nanoparticle length scale on the intermonomer correlations which can result in qualitative distortion of the correlation hole. As ϕ increases, the local monomer packing correlations are weakly perturbed out to a distance of $\sim 2-4d$, although a reduction of oscillatory order is clearly visible in Figure 2b. Beyond this local order regime there are large variations relative to the pure melt, with first a net excess of polymer, followed by a large depletion of polymer. Perturbation of pure melt packing continues for a distance determined by ϕ and the nanoparticle size asymmetry ratio. To the best of our knowledge, this many-body effect has only been previously observed in the Monte Carlo simulations of Vacatello.[12] At high filler volume fractions the polymer is strongly perturbed in a manner that is rather generic.

Secondary consequences of adding fillers to a dense melt are associated with quantitative modification of the amplitude of preexisting features of $g_{pp}(r)$. On the basis of many calculations (not presented), we find the extent of nanoparticle imprintation can range from a few ($\sim 1-2$) filler diameters (for relatively

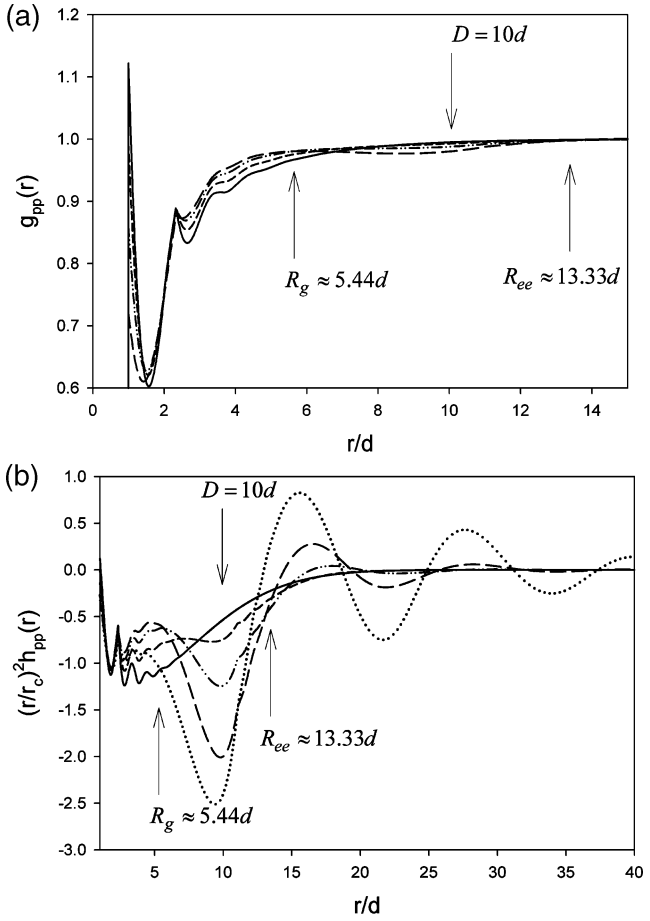

Figure 2. (a) Variation of the monomer−monomer pair correlation function with nanoparticle volume fraction, ϕ, for $D/d = 10$, $\alpha = 0.25$, and $\epsilon_{pc} = 1.0$, with $\phi = 0$ (solid), 0.12 (short dash), 0.24 (dash−dot−dot), and 0.36 (long dash). The polymer radius of gyration and end-to-end distance, and filler diameter, are indicated. (b) Correlated component of the monomer−monomer pair correlation function weighted by the surface area factor for the same systems as (a). Additionally, the dotted curve is for the $\phi = 0.36$, $\alpha = 1.0$ system.

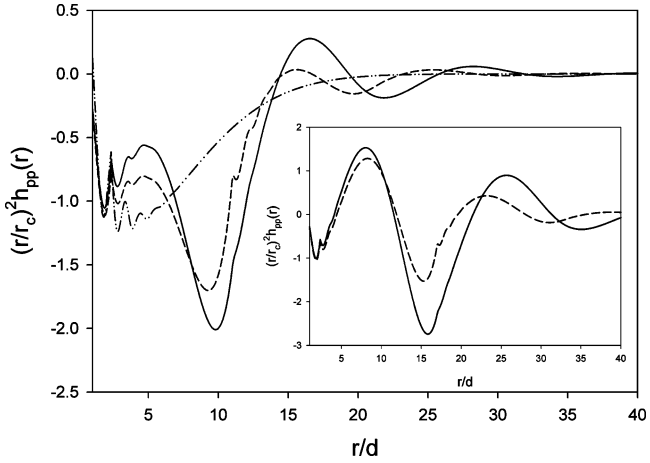

Figure 3. Weighted polymer total pair correlation function for the system with $D/d = 10$ and $\alpha = 0.25$ with $\phi = 0$ for $\epsilon_{pc} = 0$ (dash−dot−dot) and $\phi = 0.36$ for $\epsilon_{pc} = 1.0$ (solid) and $\epsilon_{pc} = 2.0$ (dash). The inset shows the $\phi = 0.36$ curves for $D/d = 16$ with the same α and ϵ_{pc} values as the main panel.

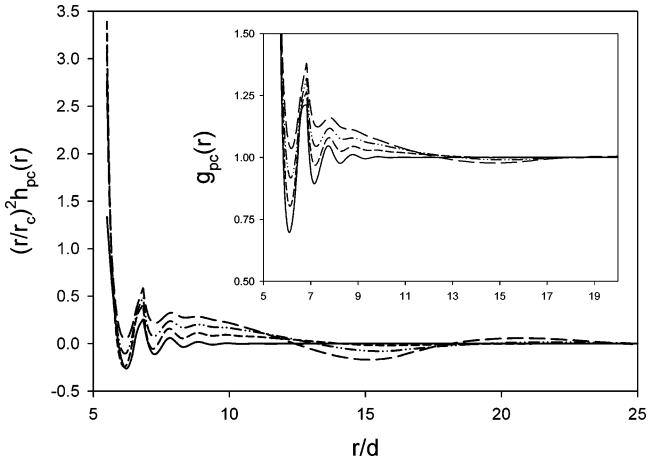

Figure 4. Weighted polymer−filler total pair correlation function for various nanoparticle volume fractions, ϕ. System variables are $D/d = 10$, $\alpha = 0.25$, $\epsilon_{pc} = 1.0$, with $\phi = 0$ (solid), 0.12 (short dash), 0.24 (dash−dot−dot), and 0.36 (long dash). Contact values are $g_{pc}(r = r_c) = 4.69$, 4.39, 4.08, and 3.76 for $\phi = 0$, 0.12, 0.24, and 0.36, respectively. Inset: same results for the pair correlation function.

low ϵ_{pc} or α as shown in Figure 2a) to many (∼4+) nanoparticle diameters (at high ϵ_{pc} or α). The reason for this variability is the extent of imprintation is influenced by the degree of polymer adsorption which increases with ϵ_{pc} and/or α. For weaker adsorption, the polymer matrix is more pliant or compressible, and larger nanoparticle scale oscillations form in $g_{pp}(r)$. If the magnitude of the monomer−filler attraction is increased, these oscillations are reduced. On the other hand, if the attraction *range* is increased, the imprinted oscillations increase in amplitude (Figure 2b).

Figure 3 shows the filler-induced perturbation of polymer packing at a fixed volume fraction increases with nanoparticle size. However, sensitivity to ϵ_{pc} appears to lessen on local scales as filler diameter increases. Perhaps this trend is due to larger particles being more locally flat and thus able to more efficiently stabilize tighter polymer−particle packing. In addition, smaller nanoparticles at fixed volume fraction have more surface area, and more of the matrix polymer is perturbed from its bulk behavior.

B. Filler−Polymer Interfacial Correlations. The interfacial pair correlations, $g_{pc}(r)$, quantify the direct effect of nanoparticles on polymer packing near filler surfaces. Figure 4 shows results for moderate polymer−particle attractions and variable filler loading that are the analogue of Figure 2. At infinite dilution, there is a strong peak at contact, followed by a region of local oscillatory layering on the few monomer length scale. As ϕ increases and polymers are more highly constrained, there is overlap and interference between the organized polymer layers around different nanoparticles. One consequence is the interfacial contact value decreases (roughly linearly) with filler volume fraction. Concurrent with this, the correlations near the particle surface rise substantially, maintaining the packing structure of the first few peaks near the nanoparticle surface before decaying slowly to zero at a monomer−filler separation of $r \approx r_c + D$. Beyond the latter separation low-amplitude oscillations again occur indicative of imprinting of the nanoparticle length scale. Note the emergence of a near plateau (with superimposed oscillations) of $r^2 h_{pc}(r)$ for $r < D = 10d$. This feature is absent in the dilute limit, and interestingly it suggests the correlated part of the monomer−particle correlations initially decays as the inverse square of separation.

The interpretations advanced above are strengthened by examining the consequences of increased attraction energy and spatial range. We refrain from presenting more figures and simply summarize our findings. For a larger $\epsilon_{pc} = 2$, the same qualitative trends are observed as in Figure 4, but the increased

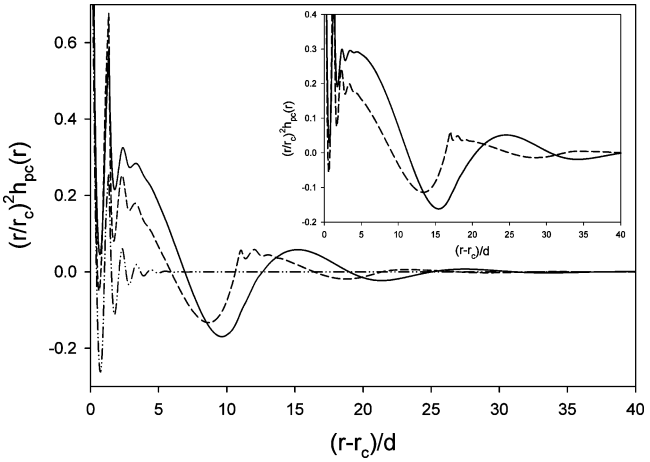

Figure 5. Weighted interfacial pair correlation function as a function of the reduced monomer−filler separation from contact for the system with $D/d = 10$, $\alpha = 0.25$ with $\phi = 0$ for $\epsilon_{pc} = 0$ (dash−dot−dot) and $\phi = 0.36$ for $\epsilon_{pc} = 1.0$ (solid) and $\epsilon_{pc} = 2.0$ (dash). The inset shows the $\phi = 0.36$ curves for $D/d = 16$ with the same α and ϵ_{pc} values as the main panel.

adsorption results in a reduction of the oscillatory features imposed by nanoparticle packing correlations. For example, the reduction of the cross-correlation contact value by ∼12% at $\phi = 0.36$ is less than in Figure 2. This supports our deduction that increasing monomer adsorption reduces the pliancy of the polymer matrix. Increasing the attraction range is found to increase the imprinting correlations on $h_{pc}(r)$, as it did for the polymer−polymer correlations in Figure 2b.

Figure 5 demonstrates that similar qualitative trends as found for the polymer correlations occur for the dependence of $h_{pc}(r)$ on nanoparticle size asymmetry ratio D/d; i.e., a change in filler diameter induces a commensurate shift in oscillation period. However, for the interfacial correlations changing nanoparticle size does not seem to significantly modify the relative amplitude (with all other system variables held constant) of the reorganization in contrast to the response of the polymer correlations (Figure 3).

C. Filler−Filler Correlations. As ϕ increases, and the polymers in the PNC rearrange, the polymer-induced modification of nanoparticle packing must self-consistently change. The intuition and trends established from our prior infinite dilution calculations[17,18] are used as a baseline to interpret this restructuring in terms of the nanoparticle PMF, $W_{cc}(r) = -k_BT \times \ln(g_{cc}(r))$. Note that large positive (negative) values of the PMF correspond to nearly zero (large peak) values of the pair correlation function.

Figure 6 shows the filler PMF analogues of Figures 2 and 3. Finite nanoparticle volume fraction effects can be substantial when the polymer matrix is relatively pliant (moderate $\epsilon_{pc}= 1$; Figure 6a), while it is significantly less if the polymer near the nanoparticle is more rigidly bound (larger $\epsilon_{pc}= 2$; Figure 6b). At infinite dilution, the PMF of the $\epsilon_{pc} = 1$ system is highly structured, with a global minimum of approximately 1 k_BT at a separation of one monomer diameter and oscillations around random packing ($W_{cc} = 0$) extending approximately four monomer diameters from contact. As ϕ is increased, the global minimum of the PMF becomes more shallow, and the proceeding minimum deepens until, at $\phi = 0.36$, the global minimum has shifted to a larger filler separation of ∼2d with a magnitude of only ∼0.5 k_BT. Additionally, a long range (∼8−10d) and weak (<0.5 k_BT) attractive tail emerges with increasing filler volume fraction which favors many-particle clustering. When ϵ_{pc} is increased to 2 and strong bridging emerges (Figure 6b),

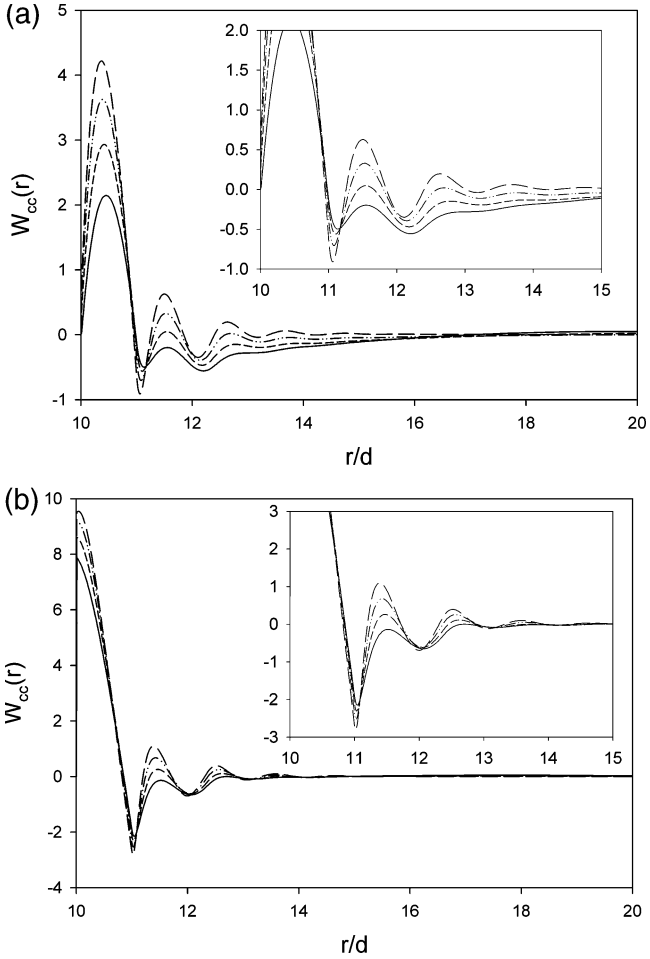

Figure 6. (a) Nanoparticle potential of mean force (in thermal energy units) for various volume fractions. System variables are $D/d = 10$, $\alpha = 0.25$, and $\epsilon_{pc} = 1$, with $\phi = 0$ (long dash), 0.12 (dash−dot−dot), 0.24 (short dash), and 0.36 (solid). Interparticle separation is in units of monomer diameter, d. Inset: expanded view of the near contact region. (b) Same as (a) but for $\epsilon_{pc} = 2$.

the filler reorganization with increasing ϕ is less pronounced. The global minimum remains fixed for all volume fractions at the infinite dilution separation of one monomer diameter, and its depth is perturbatively reduced. The primary many-particle effect is a strong reduction of repulsive barriers, which is reminiscent of the formation of the long attractive tail for the smaller $\epsilon_{pc} = 1$ system, but no true long-ranged attractive tail emerges.

Figure 7a shows results for a longer range attraction of $\alpha = 0.5$ and $\epsilon_{pc} = 1$, corresponding to organization intermediate between bound layer formation and bridging in the dilute limit.[18] As ϕ increases, the fine scale oscillations in the PMF disappear due to destructive interference of polymer layering around different particles, and a relatively long range, shallow attractive tail grows in. For the longest range (softest) filler−monomer attraction ($\alpha = 1$), interesting changes of particle packing emerge as ϕ increases. The $\epsilon_{pc} = 1$ system has a *purely repulsive* infinite dilution PMF and no fine-scale bridging structure to reorganize (Figure 7b). However, as the nanoparticle concentration increases, the filler PMF changes dramatically and acquires a *net attractive* character of an explicitly many-body origin with a characteristic interfiller separation of ∼4d. Additionally, a longer range oscillation with a repulsive barrier emerges which is not present for the analogous systems of Figures 6 and 7a.

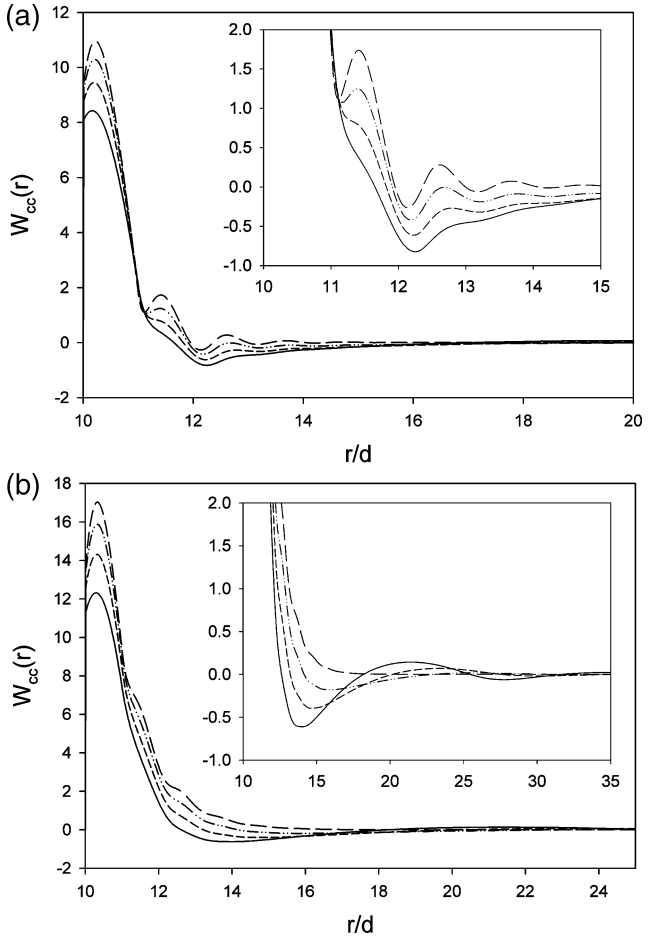

Figure 7. (a) Same as Figure 6a but for a longer range monomer−filler attraction of $\alpha = 0.5$. (b) Same as (a) but for the longest range attraction of $\alpha = 1$.

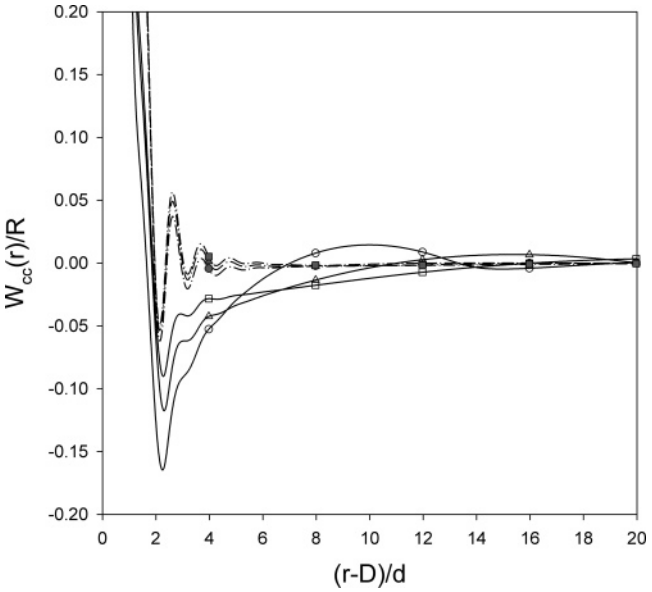

Figure 8. Filler potential of mean force divided by the particle radius (in units of d) as a function of intersurface separation for three size asymmetry ratios. System variables are $\alpha = 0.5$, $\epsilon_{pc} = 1.0$, and $\phi = 0.04$ (dash−dot−dot) and 0.36 (solid) with $D/d = 10$ (circle), 16 (triangle), and 24 (square).

Figure 8 examines the effect of filler size by plotting the PMF reduced by the filler radius for three nanoparticle diameters. Under dilute conditions we have previously shown[17,18] the PMF linearly scales extremely well with D/d ($\bar{W}_{cc} \equiv W_{cc}/R$ collapses) for $D/d > 6-7$, in analogy with polymer-induced forces between two flat surfaces. Figure 8 demonstrates that even at a very small ϕ (0.04) corrections to the infinite dilution scaling exist. At high volume fractions deviations from the linear D/d scaling are of a *qualitative* nature, and the primary attraction well exhibits a much weaker size dependence. The breadth of the longer range attractive well depends on D/d, with larger size asymmetry ratio systems having longer ranged (and shallower) attractive wells, and a subsequent small repulsive barrier. These trends are likely due to local monomer scale packing features being increasingly averaged over as filler surface area increases.

D. Summary. Increasing filler volume fraction has a profound effect on the structure of the polymer matrix, causing reorganization to occur on a length scale commensurate with the diameter of the nanoparticles. The oscillatory aspects of the reorganization can extend over several filler diameters. The interfacial correlations respond to increased nanoparticle volume fraction by suppressing the contact layer of polymer. However, a major excess of monomer builds up near the particle surface, with $h_{pc}(r)$ decaying in a roughly $\sim 1/r^2$ fashion with imprinted D/d scale oscillations for longer distances. For both the polymer and interfacial correlations, the magnitude of these oscillations is larger for smaller values of ϵ_{pc} due to the enhanced ability to rearrange polymer when there is less adhesion between monomers and nanoparticles. Increased filler volume fraction also substantially changes nanoparticle packing, inducing a transition from highly bridged or sterically stabilized organization in the infinite dilution limit, to more diffuse liquidlike packing as ϕ increases. The presence of many-body interference effects due to multiple nanoparticles largely destroys the fine-scale features characteristic of the infinite dilution filler PMF, replacing them with longer ranged, shallow attractive wells and sometimes a repulsive barrier. If the interfacial adhesion strength is increased, this effect is substantially reduced due to the locally less compressible nature of the polymer chains near nanoparticles.

IV. Partial Collective Structure Factors

In this section, calculations of the positive-definite "diagonal" partial collective structure factors ($S_{jj}(k)$) of the polymer and filler subsystems are presented. These functions clearly reveal the length scales over which concentration fluctuations are most strongly correlated. While such information is in principle encoded in the real-space correlation functions, Fourier space structure factors vividly expose changes in collective organization of the PNC, especially on larger length scales. They also are potentially measurable via small- and wide-angle X-ray or neutron scattering.[25,26]

A. Polymer Structure Factor. As shown in the inset of Figure 9, the structure factor of a dense one-component homopolymer melt has only two notable features: the value of the dimensionless isothermal compressability $S_{pp}(k = 0)$ and the monomer scale "local cage" peak at $kd \approx 2\pi$, the location and intensity of which quantifies the characteristic length scale and coherence, respectively, of monomer packing. Both these aspects of $S_{pp}(k)$ are expected to be modified by the nanoparticle-induced reorganization of the polymer matrix. In addition, qualitatively new features appear in the collective polymer structure factor due to volume exclusion constraints and interfacial cohesion.

Figure 9 is the analogue of Figures 2 and 3 and shows that with increasing nanoparticle volume fraction there is a somewhat complex effect on the polymer osmotic compress-

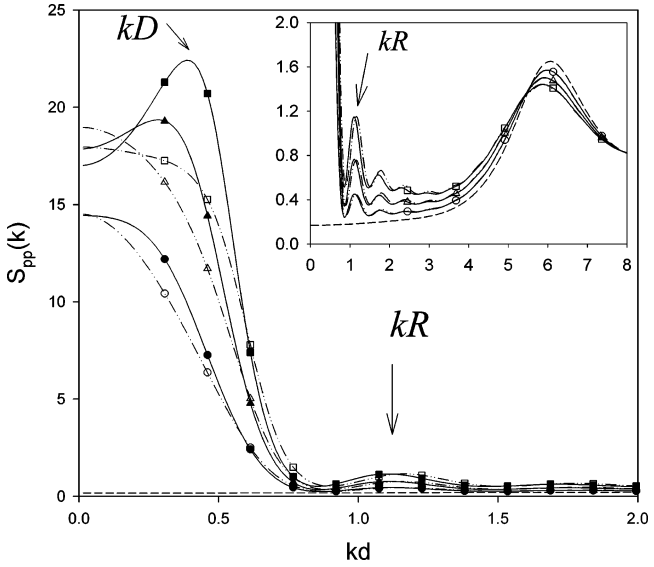

Figure 9. Dimensionless polymer collective structure factor as a function of wavevector nondimensionalized by the monomer diameter. The main graph emphasizes the small wavevector regime, and the inset highlights the entropic excluded volume peak and local cage region where wavevector is scaled by the filler radius. The arrows indicate where kD and $kR \sim 2\pi$. System variables are $D/d = 10$, $\alpha = 0.25$, and $\epsilon_{pc} = 1$ (solid) and 2 (dash−dot−dot) with $\phi = 0.0$ (unmarked, dashed), 0.12 (circles), 0.24 (triangles), and 0.36 (squares).

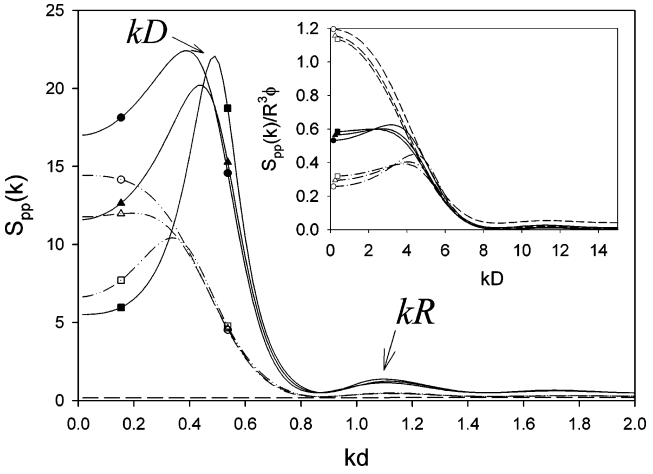

Figure 10. Variation of the polymer structure factor with increasing interfacial attraction range, α. The main graph emphasizes the $k = 0$ limit (osmotic compressibility) and bound layer peak. The arrows indicate where kD and $kR \sim 2\pi$. System variables are $D/d = 10$, $\epsilon_{pc} = 1$, and $\phi = 0.12$ (dash−dot−dot) and 0.36 (solid), with $\alpha = 0.25$ (circle), 0.5 (triangle), and 1 (square). The inset demonstrates the near collapse of the structure factor when normalized by a factor of $R^3\phi$ for systems with $\epsilon_{pc} = 1$, $\alpha = 0.5$, and $\phi = 0.04$ (short dash), 0.20 (solid), and 0.36 (dash−dot) with $D/d = 10$ (circle), 16 (triangle), and 24 (square).

ibility $S_{pp}(k = 0)$. Initially, $S_{pp}(k = 0)$ increases with ϕ due to the voids being created in the polymer matrix and the corresponding long-range (relative to the monomer scale) polymer concentration fluctuations. As more nanoparticles are introduced, $S_{pp}(k = 0)$ initially continues to grow but now in a sublinear manner since the void spaces become less random as nanoparticles acquire a liquidlike ordering. Ultimately, this trend *reverses*, and $S_{pp}(k = 0)$ *decreases* with increasing filler loading. Concurrent with this reversal is the emergence of a new peak at a wavevector that scales roughly as $kd \sim 2\pi/(D + \Delta)$, where Δ is the "bound polymer layer" thickness.[18] This bound layer, or in analogy with block copolymers "microphase-separation-like",[32,33] peak is associated with the layer of highly intermolecularly correlated adsorbed polymer which is organized in a manner distinct from the "bulk" matrix homopolymer. Its formation is dictated not only by filler volume fraction but also by the interfacial cohesion range and strength since both these quantities influence how tightly the polymer adheres to and packs near the nanoparticle.[18]

A new feature in $S_{pp}(k)$ also emerges at wavevectors between the bound layer and local cage peaks, as shown in detail in the inset of Figure 9. Specifically, a much weaker, but omnipresent, set of peaks occur at values of kR of order 2π, where R is the nanoparticle radius. This series of peaks was previously predicted and discussed for polymer−colloid suspensions.[34] It is related to purely excluded volume induced correlations due to packing of the monomers of even a single chain (dilute regime) at the surface of a hard sphere. Its mathematical form is akin to the classic Bessel function form factor of a continuous, constant density solid sphere.[34] Unlike the bound layer or microphase-like peak, these "excluded volume" peaks are relatively uninteresting since they are essentially unperturbed by changes in system attraction variables. Since, to a first approximation, its origin is the exclusion of a polymer from a *single* isolated sphere, the only substantial dependence is on R. Finally, the inset of Figure 9 shows the local cage peak shifts to lower wavevector (longer distance) and decreases in intensity with ϕ. This indicates that the monomer scale cage modestly expands and disorders due to the incorporation of nanoparticles in the polymer melt. This trend is the Fourier space analogue of the filler-induced suppression of local oscillatory packing correlations in $g_{pp}(r)$, as shown in Figure 2b.

Figure 10 shows the response of the collective polymer concentration fluctuations to increasing monomer−particle attraction range for low ($\phi = 0.12$) and high ($\phi = 0.36$) filler loading. For $\phi = 0.12$, the ability of increased interfacial cohesion to enhance bound layer organization is clearly visible, with the $\alpha = 0.25$ system showing no discernible peak, while the $\alpha = 1$ system clearly has "captured" a bound polymer layer. Similarly, at $\phi = 0.36$ the higher α system displays narrower, better defined bound layer peaks. Interestingly, however, the relative magnitude of these bound layer peaks is a nonmonotonic function of α. Whether this indicates some fundamental packing limitation due to the different length scales of organization, or is simply a remnant of residual disorder at lower wavevectors arising from the fact that the $\alpha = 0.25$ system has a weakly bound polymer layer, is difficult to determine.

A comparison of Figures 9 and 10 highlights an interesting trend in the bound layer evolution. At $\epsilon_{pc} = 1$, increasing α leads to a more defined bound layer peak, implying that increased interfacial cohesion enhances the formation of a discernible polymer layer. However, increasing the attraction strength (which *also* increases cohesive energy) can diminish (or outright destroy) the bound layer peak. In general, as ϵ_{pc} is increased, the system is expected to progress across phase diagram from fluid−fluid demixing, through sterically stabilized miscibility, and into a networked state of organization,[19] as indicated in Figure 1. The diminishing of the bound layer peak with increased attraction is thus a precursor of the miscible system approaching the bridging induced network spinodal. However, this trend is not universal and depends on the precise manner the network spinodal is approached. For example, as discussed elsewhere,[35] if ϵ_{pc} is held fixed at a rather high value and the filler volume fraction is increased, then the microphase peak can actually *intensify* simultaneously with a strong growth

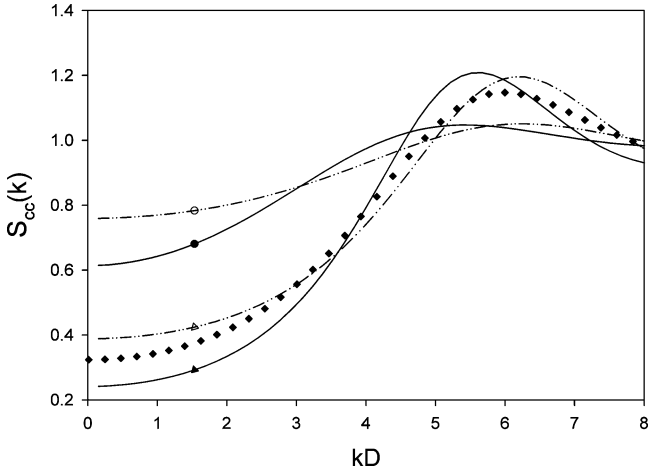

Figure 11. Nanoparticle collective structure factor as a function of wavevector nondimensionalized by particle diameter for several filler volume fractions (ϕ) and interfacial cohesion strengths (ϵ_{pc}). System variables are $D/d = 10$ and $\alpha = 0.25$ for $\epsilon_{pc} = 1$ (solid) and 2 (dash−dot−dot) with $\phi = 0.12$ (circles) and 0.36 (triangles). The solid diamonds are the corresponding pure hard-sphere fluid structure factor with $\phi = 0.36$ (see text).

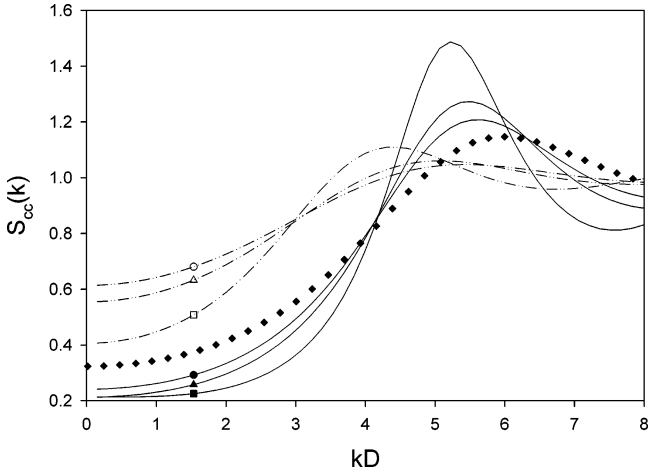

Figure 12. Nanoparticle collective structure factor for several filler−monomer attraction ranges, α. System variables are $D/d = 10$, $\epsilon_{pc} = 1$, $\phi = 0.12$ (dash−dot−dot), and 0.36 (solid) with $\alpha = 0.25$ (circle), 0.5 (triangle), and 1 (square). The series of solid diamonds represents the structure factor for a pure hard sphere fluid with $\phi = 0.36$ ($\phi_s = 0.144$).

of the $k = 0$ scattering intensity (osmotic compressibility), resulting in a $S_{pp}(k)$ with two small angle peaks reminiscent of microemulsions where large-amplitude concentrations fluctuations at zero and finite wavevector coexist.[36]

Both the excluded volume and local cage peaks show little or no variability with increasing attraction range. These primarily entropic (excluded volume) structural features are insensitive to changes in attraction range or strength, being modified only by ϕ and, for the excluded volume peak, the size asymmetry ratio, D/d.

The dependence of $S_{pp}(k)$ at low wavevectors on nanoparticle size and volume fraction has also been studied (inset of Figure 10). Over a wide range of filler volume fractions the $S_{pp}(k)$ collapse reasonably well on the mesoscopic scale ($kR < 1$) when normalized by $R^3\phi$. This approximate superposition can be rationalized by realizing that the nanoparticles are organizational centers for both the bound layer and excluded volume peaks. There are small deviations from this behavior for the latter if R becomes so small that the nanoparticles no longer efficiently organize the near surface packing of monomers. The bound layer peaks, on the other hand, deviate more strongly in *shape*, and smaller nanoparticles have more well-defined peaks at nonzero wavevectors.

B. Filler Structure Factor. Compared to the multiple novel features of the collective polymer structure factors, the nanoparticle structure factors in miscible mixtures are far simpler and display no qualitatively new small angle features. However, distinctive changes in the local cage peak do emerge with increasing filler volume fraction, and the filler osmotic compressibility $S_{cc}(k = 0)$ can either increase or follow a nonmonotonic dependence with particle volume fraction depending on the proximity of the mixture to a spinodal boundary. To better understand the role of polymer mediation of filler packing, it is instructive to compare the nanoparticle structure factors to an appropriate hard-sphere fluid reference system with the same space-filling volume fraction as the filler. For such comparisons, the proper space-filling *packing* fraction (ϕ_s) of the hard-sphere reference system is $\phi_s \equiv \phi\eta = \phi(0.4)$.

Figure 11 shows a representative example for $D/d = 10$ and $\alpha = 0.25$ at moderate and high filler volume fractions. At the lower ϵ_{pc} value, $S_{cc}(k)$ has a cage peak that is shifted to smaller wavevectors relative to its reference hard-sphere fluid. This indicates that the cage is expanded due to the presence of the bound polymer layers or equivalently the filler has a larger effective radius than its bare value.[18] However, for the more cohesive $\epsilon_{pc} = 2$ system the structure factor peak is shifted to slightly *higher* wavevectors than the reference hard-sphere fluid. This indicates a *smaller* mean nanoparticle separation, consistent with the relatively tightly bridged configuration deduced from the analogous real space calculations of section III and prior work.[18]

The magnitude of the wide angle structure factor peak quantifies the degree of local filler spatial order. In a dense homopolymer melt, the binding of polymer to nanoparticles has the net effect of increasing the apparent filler radius.[18] Figure 11 demonstrates that even for the nonrepulsive, bridging states there is a modest tendency to more highly organize the nanoparticles due to the presence of the dense polymer matrix, resulting in a larger effective filler diameter. When the interfacial attraction range is increased, the thickness of the bound layer grows, leading to a significantly larger effective volume of the nanoparticle. Figure 12 demonstrates this effect for $\epsilon_{pc} = 1$ at the same volume fractions as in Figure 11. The effective filler volume enhancement of the $\alpha = 1$ system is striking, with $S_{cc}(k)$ looking like a significantly denser and less compressible hard-sphere fluid. If the nanoparticle diameter is increased, the effective volume fraction enhancement due to the bound layer becomes smaller, and hence the differences between the PNC $S_{cc}(k)$ and its hard-sphere reference fluid analogue are less.

Figure 13 examines in detail the phenomenon of increased effective filler volume fraction for the $\alpha = 1$ system which has the largest bound layer. A particle volume fraction of 0.36 corresponds to a total packing fraction of only 0.144. The analogous results for a pure hard-sphere fluid at a packing fraction of 0.353 are also shown. The comparable heights of the cage peak, and significant shift to smaller wavevectors, indicate the ability of the polymer matrix to induce a high degree of filler ordering even with a significant gap between nanoparticles due to the thermodynamically stable adsorbed polymer layers. The upturn in $S_{cc}(k = 0)$ for the $\epsilon_{pc} = 1$ system indicates the onset of filler clustering.

C. Clustering and Phase Transition Precursors. Although PRISM theory applies only to the homogeneous equilibrium liquid state, some of the unusual structure factor features discovered are precursors of clustering and phase separation.

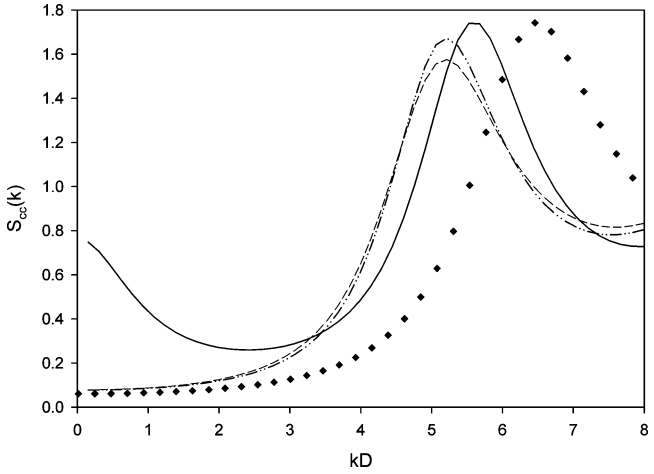

Figure 13. Nanoparticle structure factor for various adhesion strengths and $D/d = 10$, $\alpha = 1$, and $\phi = 0.36$ with $\epsilon_{pc} = 0.25$ (short dash), 0.5 (dash−dot−dot), and 1 (solid). The shift in the local cage peak and upturn of the $\epsilon_{pc} = 1$ curve signals the onset of local clustering. The solid diamonds represent the structure factor for a pure hard-sphere fluid with $\phi_s = 0.352$.

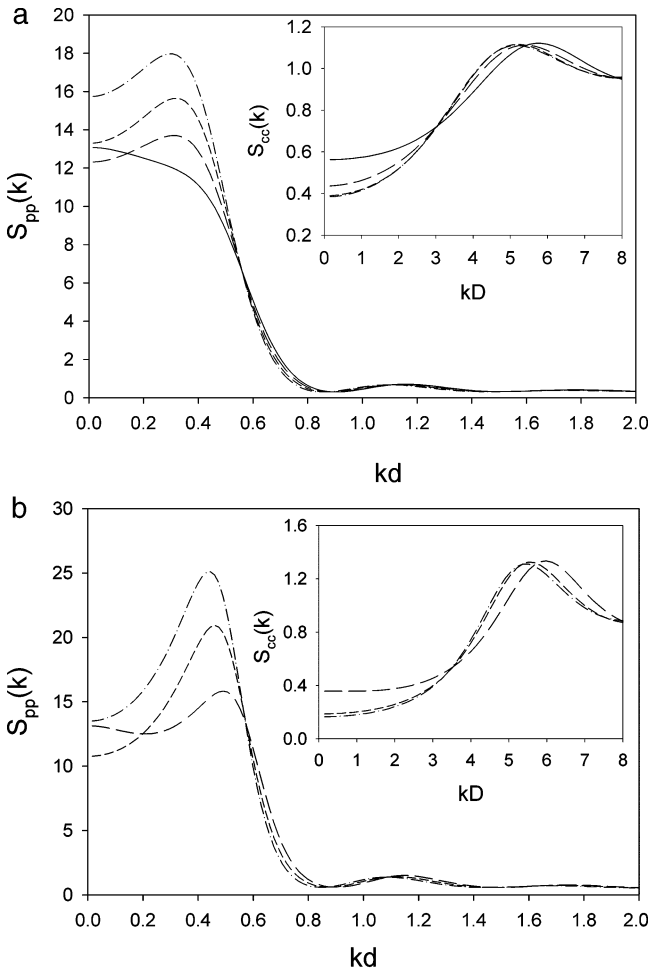

Figure 14. (a) Polymer structure factor for a $D/d = 10$, $\phi = 0.20$, and $\alpha = 0.5$ system for increasing $\epsilon_{pc} = 0.5$ (dash−dot), 1 (short dash), 1.5 (long dash), and 2 (solid). The distinctive nonmonotonic changes are suggestive of a miscible-to-bridging transition with increasing ϵ_{pc}. The inset is the corresponding nanoparticle collective structure factors. (b) Same as (a) (except $\epsilon_{pc} = 2$ is omitted) for a very high filler volume fraction of $\phi = 0.40$.

Examples are given in Figure 14 for two filler volume fractions and increasing cohesion strengths. The polymer dimensionless osmotic compressibility ($S_{pp}(k = 0)$) is a *nonmonotonic* function of monomer−filler attraction (ϵ_{pc}) at both $\phi = 0.2$ and 0.4. For the lower volume fraction (Figure 14a) at $\epsilon_{pc} = 0.5$ the signature of the bound layer is clearly present, and as ϵ_{pc} increases, this microphase-like peak and the osmotic compressibility both decrease in intensity. However, as $\epsilon_{pc} \rightarrow 2$, the shift of $S_{pp}(k = 0)$ with interfacial cohesion reverses, and the bound peak disappears. The logical explanation for this sequence of behavior is the evolution from a miscible structure with discrete bound layers to a tightly bridged network type of organization where the adsorbed polymers are shared between multiple fillers, thereby blurring the scattering signature of the bound layers. Interestingly, while there are pervasive changes at low wavevector in the polymer structure factor, the excluded volume low angle peak and local cage structure feature are essentially unchanged (inset of Figure 14b). The inset of Figure 14a shows analogous changes (though small) of the nanoparticle collective structure factor occur including an increase of $S_{cc}(k = 0)$ and a shift of the cage peak toward larger wavevectors as a consequence of bridging becoming statistically important.

Figure 14b shows the behavior at a very high filler volume fraction ($\phi = 0.4$). Note the clear shift of the bound layer peak to higher wavevector with increasing interfacial cohesion strength and the microemulsion-like[36] coexistence of peaks at $k = 0$ and nonzero wavevector in the small angle regime for the $\epsilon_{pc} = 1.5$ system. Overall, the qualitative trends are similar to the lower volume fraction system of Figure 14a.

D. Summary. Increasing filler volume fraction has a profound effect on the polymer matrix correlations, resulting in several novel modifications of the collective polymer structure factor. At low wavevectors there is an increase in the polymer osmotic compressibility due to the necessity of incorporating sufficient void space to accommodate the nanoparticles. In addition, with sufficient interfacial attraction strength, range, and/or filler volume fraction, the polymer becomes highly organized around the nanoparticles. This leads to the emergence of a large bound layer or microphase-separation-like scattering peak at $kD \sim 2\pi$. A series of smaller scattering peaks also emerge at kR of order unity due to (primarily) entropic or excluded volume effects of placing monomers near the nanoparticle surface. Finally, the polymer local cage structure is perturbed, with fillers suppressing local cage coherence and shifting the monomer packing to a more open or diffuse arrangement. Increased filler volume fraction also serves to substantially rearrange the way in which nanoparticles collectively pack. The modifications are largely quantitative, not qualitative, relative to a hard- sphere fluid, and depend on the relative importance of sterically stabilized (bound layer) vs bridging packing organization.

V. Bulk Modulus

PRISM theory also enables the calculation of an interesting thermodynamic property: the mixture bulk modulus, K_B, given by[37]

$$\beta K_B = \frac{\rho_p}{N} - \rho_p{}^2\tilde{C}_{pp} + \rho_c - \rho_c{}^2\tilde{C}_{cc} - 2\rho_p\rho_c\tilde{C}_{pc} \qquad (9)$$

where ρ_p and ρ_c are the monomer and filler number densities, respectively, and $\tilde{C}_{ij} \equiv C_{ij}(k = 0)$. The bulk modulus is inversely proportional to the isothermal compressibility and quantifies the amplitude of *total* density fluctuations in the mixture.

Figure 15 presents representative results for the bulk modulus normalized by its pure polymer melt value for $D/d = 10$ and a variety of system parameters. The behavior across all system variables (attraction strength and range and D/d (not shown)) is extremely similar, always corresponding to a monotonic

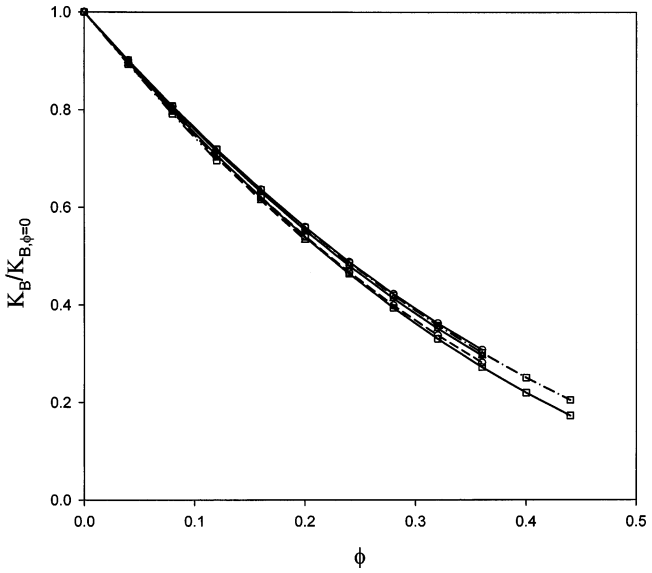

Figure 15. Total bulk modulus of the PNC normalized by its pure polymer melt value as a function of filler volume fraction for multiple adhesion strengths (ϵ_{pc}) and attraction ranges (α). System variables are $D/d = 10$, with $\epsilon_{pc} = 0.5$ (dash−dot), 1 (solid), 1.5 (dash−dot−dot), and 2 (short dash) and $\alpha = 0.25$ (circle), 0.5 (triangle), and 1 (square).

decrease, or softening, of the bulk modulus with increasing filler loading. Hence, at *constant mixture total packing fraction* the addition of particles to a dense polymer melt enhances the compressibility or total density fluctuations. This filler-induced reduction of the bulk modulus is consistent with the general finding of a reduced local polymer packing order as indicated by weaker oscillatory features in $g_{pp}(r)$ (Figure 2b) and a less intense and shifted wide angle peak in $S_{pp}(k)$ (Figure 9). The decay of the modulus is weakly sublinear with increasing filler volume fraction. Despite the large differences seen in structural correlations as α, ϵ_{pc} or D/d is varied, the bulk modulus remains invariant to within 10% or less. We are not aware of published experiments or simulations that have determined the bulk modulus of nanocomposites.

VI. Summary and Discussion

The three coupled nonlinear PRISM integral equations have been numerically solved for mixtures of hard-sphere nanoparticles and adsorbing polymer for a broad range of system parameters. By necessity, the calculations are only performed in the miscible state although the behavior as the two distinct spinodal curves are approached has been explored. Detailed summaries of the key findings, trends, and physical picture for the real space correlations and collective structure factors have been given at the end of sections III and IV, respectively. We hope these results stimulate attempts to use small-angle X-ray and/or neutron scattering, and many-particle computer simulations, to test our Fourier and real space predictions, respectively.

A particularly interesting finding is that for values of α and ϵ_{pc} which correspond to steric stabilization in the infinite dilution state many-particle effects can induce net attractions and filler clustering. This suggests a tendency for many-particle effects to further decrease the miscibility relative to our prior virial based calculations of phase boundaries.[19] Ongoing computational work involves the application of more powerful numerical algorithms to solve the nonlinear integral equations at very high filler volume fractions and close enough to phase separation that the full many-particle spinodal boundaries can be determined.[35]

At a more conceptual and method development level, efforts are underway to generalize the equilibrium theory in three directions: (i) polymer nanocomposites composed of nonspherical fillers (e.g., disks, rods, nanocubes, "molecules"), (ii) dense melts and concentrated solutions of spherical nanoparticles carrying grafted polymers, and (iii) mixtures of chemically matched homopolymers and hairy fillers. Finally, the availability of quantitative structural correlations for polymer nanocomposites provides a foundation for the development of predictive microscopic theories of their dynamics including the questions of filler diffusion, viscoelasticity, glass formation, and physical aging. The issue of depletion and bridging induced phase separation being "preempted" by nonequilibrium gelation will be addressed elsewhere.[35]

Acknowledgment. This work was supported by the Nanoscale Science and Engineering Initiative of the National Science Foundation under NSF Award DMR-0117792 and the U.S. Department of Energy BES program via Oak Ridge National Laboratory. We thank Lisa Hall, Sanat Kumar, and Michael Mackay for discussions and Lisa Hall for valuable comments on the manuscript.

References and Notes

(1) Wang, M.-J. *Rubber Chem. Technol.* **1998**, *71*, 520; **1999**, *72*, 430.
(2) Ajayan, P. M.; Schadler, L. S.; Braun, P. V. In *Nanocomposite Science and Technology*; Wiley-VHC: Weinheim, 2003; p 77.
(3) Vieweg, S.; Unger, R.; Heinrick, G.; Donth, E. *J. Appl. Polym. Sci.* **1999**, *73*, 495.
(4) Ash, J.; Schadler, L. S.; Siegel, R. W. *Mater. Lett.* **2002**, *55*, 83. Ash, J.; Seigel, R. S.; Schadler, L. S. *Macromolecules* **2004**, *37*, 1358. Bansal, A.; Yang, H.; Li, C.; Benicewicz, B. C.; Kumar, S. K.; Schaler, L. S. *J. Polym. Sci., Polym. Phys.* **2006**, *44*, 2944.
(5) Mackay, M. E.; Dao, T. T.; Tuteja, A.; Ho, D. L.; van Horn, B.; Kim, H-C.; Hawker, C. J. *Nat. Mater.* **2003**, *2*, 762, Mackay, M. E.; Tuteja, A.; Duxbury, P. M. *Science* **2006**, *311*, 1740.
(6) Huber, G.; Vilgis, T. A. *Macromolecules* **2002**, *35*, 9204.
(7) Doxstakis, M.; Chen, Y. L.; dePablo, J. J. *J. Chem. Phys.* **2005**, *123*, 034901.
(8) Patel, R.; Egorov, S. A. *J. Chem. Phys.* **2006**, *123*, 144916; **2004**, *121*, 4987; **2002**, *123*, 144916.
(9) Salaniwal, S.; Kumar, S. K.; Douglas, J. F. *Phys. Rev. Lett.* **2002**, *89*, 258301.
(10) Starr, F. W.; Schroeder, T. B.; Glotzer, S. C. *Macromolecules* **2002**, *35*, 4481.; *Phys. Rev. E* **2001**, *64*, 021802.
(11) Starr, F. W.; Douglas, J. F. *J. Chem. Phys.* **2003**, *119*, 1777.
(12) Vacatello, M. *Macromolecules* **2001**, *34*, 1946; **2002**, *35*, 8191.
(13) Smith, J. S.; Bedrov, D.; Smith, G. D. *Compos. Sci. Technol.* **2003**, *63*, 1599. Bedrov, D.; Smith, G. D.; Smith, J. S. *J. Chem. Phys.* **2003**, *119*, 10438.
(14) Desai, T.; Keblinski, P.; Kumar, S. K. *J. Chem. Phys.* **2005**, *122*, 134910.
(15) Yethiraj, A.; Hall, C. K.; Dickman, R. *J. Colloid Interface Sci.* **1992**, *151*, 102. Khalatur, P. G.; Zherenkova, L.; Khoklov, A. R. *Physica A* **1997**, *247*, 205.
(16) Dickman, R.; Yethiraj, A. *J. Chem. Phys.* **1994**, *100*, 4683.
(17) Hooper, J. B.; Schweizer, K. S.; Desai, T. G.; Koshy, R.; Keblinski, P. *J. Chem. Phys.* **2004**, *121*, 6986.
(18) Hooper, J. B.; Schweizer, K. S. *Macromolecules* **2005**, *38*, 8858.
(19) Hooper, J. B.; Schweizer, K. S. *Macromolecules* **2006**, *39*, 5133.
(20) Zhao, L.; Li, Y. G.; Zhong, C.; Mi, J. *J. Chem. Phys.* **2006**, *124*, 0144913.
(21) Zhao, L.; Li, Y. G.; Zhong, C. *J. Chem. Phys.* **2007**, *126*, 014906.
(22) Ganesan, V.; Prymitsyn, V.; Surve, M.; Narayanan, B. *J. Chem. Phys.* **2006**, *124*, 221102.
(23) Prymitsyn, V.; Ganesan, V. *J. Rheol.* **2006**, *50*, 1655; *Macromolecules* **2006**, *39*, 844.
(24) Schweizer, K. S.; Curro, J. G. *Adv. Chem. Phys.* **1997**, *98*, 1. Honnell, K.; Curro, J. G.; Schweizer, K. S. *Macromolecules* **1990**, *23*, 3496.
(25) Botti, A.; Pychout-Hintzen, W.; Richter, D.; Urban, V.; Straube, E. *J. Chem. Phys.* **2006**, *124*, 174908.
(26) Sen, S.; Xie, Y.; Kumar, S. K.; Yang, H.; Bansal, A.; Ho, D. L.; Hall, L.; Hooper, J. B.; Schweizer, K. S. *Phys. Rev. Lett.* **2007**, *128*, 128302.

(27) Doi, M; Edwards, S. F. In *Theory of Polymer Dynamics*; Oxford University Press: New York, 1986.
(28) Chandler, D.; Andersen, H. C. *J. Chem. Phys.* **1972**, *57*, 1930. Chandler, D. In *Studies in Statistical Mechanics*; Montroll, E. W., Lebowitz, J. L., Eds.; North-Holland: Amsterdam, 1982; p 274.
(29) Hansen, J. P.; McDonald, I. R. In *Theory of Simple Liquids*; Academic: London, 1986.
(30) Koshy, R.; Desai, T. G.; Keblinski, P.; Hooper, J.; Schweizer, K. S. *J. Chem. Phys.* **2002**, *117*, 1893.
(31) deGennes, P. G. *Scaling Concepts in Polymer Physics*; Cornell University Press: Ithaca, NY, 1976.
(32) Bates, F. S.; Fredrickson, G. H. *Annu. Rev. Phys. Chem.* **1990**, *41*, 525.
(33) Leibler, L. *Macromolecules* **1980**, *13*, 1602.
(34) Fuchs, M.; Schweizer, K. S. *J. Phys.: Condens. Matter* **2002**, *14*, R239.
(35) Hall, L.; Schweizer, K. S., manuscript in preparation.
(36) *Micelles, Membranes, Microemeulsions and Monolayers*; Gelbart, W., BenShaul, A., Roux, D., Eds.; Springer: New York, 1994.
(37) Curro, J. G.; Schweizer, K. S. *Macromolecules* **1991**, *24*, 6736.

MA071147E